

BASIC RESEARCH PAPER

## Anti-aging treatments slow propagation of synucleinopathy by restoring lysosomal function

Dong-Kyu Kim<sup>a,b</sup>, Hee-Sun Lim<sup>b,#</sup>, Ichiro Kawasaki<sup>c</sup>, Yhong-Hee Shim<sup>c</sup>, Nishant N. Vaikath<sup>d</sup>, Omar M. A. El-Agnaf<sup>e</sup>, He-Jin Lee<sup>f</sup>, and Seung-Jae Lee<sup>a</sup>

<sup>a</sup>Department of Biomedical Sciences and Neuroscience Research Institute, Seoul National University College of Medicine, Seoul, Korea; <sup>b</sup>Department of Biomedical Science and Technology, Konkuk University, Seoul, Korea; <sup>c</sup>Department of Bioscience and Biotechnology and Institute of KU Biotechnology, Konkuk University, Seoul, Korea; <sup>d</sup>Department of Biochemistry, College of Medicine and Health Science, United Arab University, Al Ain, United Arab Emirates; <sup>e</sup>Neurological Disorders Center, Qatar Biomedical Research Institute (QBRI), and College of Science and Engineering, Hamad Bin Khalifa University (HBKU), Education City, Qatar Foundation, Doha, Qatar; <sup>f</sup>Department of Anatomy, School of Medicine, Konkuk University, Seoul, Korea

### ABSTRACT

Aging is the major risk factor for neurodegenerative diseases that are also associated with impaired proteostasis, resulting in abnormal accumulation of protein aggregates. However, the role of aging in development and progression of disease remains elusive. Here, we used *Caenorhabditis elegans* models to show that aging-promoting genetic variations accelerated the rate of cell-to-cell transmission of SNCA/ $\alpha$ -synuclein aggregates, hallmarks of Parkinson disease, and the progression of disease phenotypes, such as nerve degeneration, behavioral deficits, and reduced life span. Genetic and pharmacological anti-aging manipulations slowed the spread of aggregates and the associated phenotypes. Lysosomal degradation was significantly impaired in aging models, while anti-aging treatments reduced the impairment. Transgenic expression of *hlh-30p::hlh-30*, the master controller of lysosomal biogenesis, alleviated intercellular transmission of aggregates in the aging model. Our results demonstrate that the rate of aging closely correlates with the rate of aggregate propagation and that general anti-aging treatments can slow aggregate propagation and associated disease progression by restoring lysosomal function.

### ARTICLE HISTORY

Received 4 January 2016  
Revised 8 June 2016  
Accepted 22 June 2016

### KEYWORDS

aggregate propagation; aging; bimolecular fluorescence complementation; *C. elegans*; lysosome; Parkinson disease; SNCA/ $\alpha$ -synuclein

### Introduction

Accumulation of specific protein aggregates is the characteristic of neurodegenerative diseases, such as Alzheimer disease (AD), Parkinson disease (PD), and amyotrophic lateral sclerosis (ALS). Proteins that are aggregated in these diseases include  $A\beta$  and MAPT/tau in AD, SNCA/ $\alpha$ -synuclein in PD, and TARDBP/TDP-43 in ALS. Protein aggregation is a consequence of impaired proteostasis, which is maintained by coordinated regulation of the protein synthesis, folding, and degradation. Mutations in protein synthesis and degradation machineries cause neurodegeneration in animal models and are often linked to human neurodegenerative diseases.

Protein aggregates in neurodegenerative diseases spread progressively from limited brain regions to larger areas as the diseases progress. In the case of PD, SNCA aggregates initially occur in the lower brain stem nuclei and olfactory bulb and sequentially spread through the ascending pathways through the upper brain stem regions to the cortical areas. Cell-to-cell transmission of protein aggregates has been suggested as the underlying mechanism for this pathological dissemination in the brains of patients with neurodegenerative diseases.<sup>1–3</sup> The details of the mechanism of cell-to-cell aggregate transmission remains elusive, however, evidence suggests that the unconventional exocytosis and subsequent

endocytosis in the neighboring cells constitute the main frame of the mechanism. Under the premise that aggregate propagation leads to the progression of disease phenotypes, the disruption of intercellular aggregate transmission is emerging as a promising strategy for stopping disease progression.<sup>4,5</sup>

Cell-to-cell transmission of protein aggregates is a 2-step process: transfer of aggregates from donor cells to recipient cells, and co-aggregation of transferred proteins and endogenous proteins.<sup>6</sup> Here, we developed *Caenorhabditis elegans* (*C. elegans*) models that utilize bimolecular fluorescence complementation (BiFC)<sup>7</sup> to exhibit fluorescence in pharyngeal muscles and their associated neurons only when SNCA proteins interact with each other transcellularly. Using these animal models, we investigated the effects of aging on cell-to-cell aggregate transmission and the mechanism underlying the aging effects.

### Results


#### Generation and characterization of the *C. elegans* model for transmission of synucleinopathy

In order to develop an animal model for convenient assay of cell-to-cell protein transmission, we produced *C. elegans*

**CONTACT** Seung-Jae Lee ✉ [sjlee66@snu.ac.kr](mailto:sjlee66@snu.ac.kr) Department of Biomedical Sciences, Seoul National University College of Medicine, 103 Daehak-ro, Jongro-gu, Seoul 03080, Korea.

Color versions of one or more of the figures in the article can be found online at [www.tandfonline.com/kaup](http://www.tandfonline.com/kaup).

<sup>#</sup>Present affiliation: Celltrion Inc., Yeonsu-gu, Incheon, Korea.

 Supplemental data for this article can be accessed on the publisher's website.

transgenic lines expressing SNCA fused to either the N-terminal or C-terminal fragment of Venus, a variant of yellow fluorescence protein (Fig. 1A). The N-terminal part of Venus (V1) was attached to the SNCA N terminus (V1S), and the C-terminal part of Venus (V2) to the C terminus of SNCA (SV2). In the *C. elegans* model, V1S was expressed in the pharynx muscle using the *myo-2* promoter ( $P_{myo-2}$ ),<sup>8</sup> and SV2 and DsRed was coexpressed in neurons connected to the pharynx using the *flp-21* promoter ( $P_{flp-21}$ )<sup>9</sup> (Fig. 1B). The presence and expression of these transgenes were verified using single-worm PCR and immunofluorescence with the anti-SNCA antibody Ab274<sup>10</sup> (Fig. S1A to D), verifying specific expressions of proteins exclusively in the intended cell types. The expression pattern of  $P_{flp-21}$  has been described<sup>9</sup> and our own marker for *flp-21* promoter activity (DsRed) also exhibited the same expression pattern, which includes expression in the ADL, ASE and ASH sensory neurons, the URA motor neurons, the MC, M2 and M4 pharyngeal neurons, and the intestine (Fig. S1E).

Expression of either V1S or SV2 alone did not produce BiFC fluorescence. However, coinjection of both constructs produced strong BiFC fluorescence in both the pharyngeal muscle and adjacent neurons, and the latter were labeled with DsRed (Fig. 1C and D; Fig. S1E and G). The data indicated that protein transmission occurred in both directions. The coexpression of  $P_{flp-21}::SV2$ -DsRed and  $P_{myo-2}::V1$  (without the SNCA gene) did not generate a BiFC signal (Fig. 1C and D; Fig. S1E), indicating that the signal was not due to nonspecific interactions between the Venus fragments. To test the specificity of the BiFC system, we generated  $P_{myo-2}::V1Q25 + P_{flp-21}::SV2$ -DsRed line, the transgenic worm expressing huntingtin exon 1 with a 25 glutamine stretch under the control of  $P_{myo-2}$  and SV2 in neurons. These worms did not exhibit BiFC signal in either pharyngeal muscle or neurons (Fig. 1D; Fig. S1E). This result validates specificity of the BiFC transgenic worms for SNCA transmission. We also established integrated transgenic lines expressing V1S and SV2-DsRed respectively, and crossed them to create an integrated double-transgenic line. As expected, neither V1S nor SV2-DsRed integrated line produced BiFC fluorescence, whereas the integrated double-transgenic line showed strong BiFC fluorescence in both the pharyngeal muscle and adjacent neurons (Fig. S1F and H). Thus, this *C. elegans* BiFC system can be utilized as an in vivo model in which both protein transfer and coaggregation between SNCA proteins derived from adjacent cells can be accurately and quantitatively analyzed in real time.

BiFC fluorescence increased as the worm aged (Fig. 1E and F), and older animals showed clumps of BiFC signal while younger ones showed mostly diffuse patterns (Fig. 1E). These data indicate that SNCA transmission is a continuous process, and that the accumulated aggregates make large inclusions later in life.

We then examined the degeneration of axonal processes from the URA motor neuron.<sup>9</sup> These nerves were intact in the wild-type N2 at d 8. Expression of SV2 in neurons caused neuritic bleb formation and nerve fragmentation in a small number of worms (Fig. 1G to K), indicating autonomous cellular toxicity of SNCA in neurons. These degenerative phenotypes were further exacerbated when V1S was expressed in the pharyngeal muscle. In the latter case, approximately 15% of nerves were completely lost (Fig. 1K). To verify nerve fragmentation, we performed 3-D reconstruction of the stacked images of nerve processes. This experiment clearly

exhibited nerve fragmentation and bleb formation (Fig. 1H). These data clearly demonstrate nonautonomous cellular effects on neuronal viability. Nerve degeneration worsened as the transgenic worms aged (Fig. 1J).

In order to assess behavioral changes due to the transmission of SNCA aggregates, we performed pharyngeal pumping analysis. The pumping rates of the wild-type N2 did not change significantly with aging until d 16. Single expression of V1S or SV2-DsRed in the pharyngeal muscle and adjacent neurons, respectively, resulted in a slight decline in pumping rates in old age (Fig. 1L and Table S1). The reduction in pumping rates of all the single expressers became significant on d 13 (Fig. 1L and Table S1). Coinjection and double integrated lines showed more severe phenotypes for pumping rates, with the decline becoming apparent as early as d 2 and progressively deteriorating as the worms aged (Fig. 1L and Table S1). In longevity assays, the single-transgenic animals showed a slightly decreased life span compared to the N2 worms, whereas the life span of the double-transgenic animals was shorter than the single-transgenic lines (Fig. 1M and Table S2). Thus, aggregate transmission and inclusion body formation, as well as the associated degenerative phenotypes, progress with aging. Comparison of the timelines indicates that death of the organism is preceded by the accumulation of BiFC signal, nerve degeneration, and a decline in pumping behavior. These results were replicated with the worms expressing untagged SNCA in the same cell types as the BiFC model (Fig. S1I to L), suggesting that the phenotypes observed in the BiFC model is attributed to SNCA.

### Effects of aging-related genetic factors on cell-to-cell SNCA transmission

Next, we examined the effects of aging-related genetic variations on aggregate transmission and the degenerative phenotypes. The BiFC SNCA constructs were injected into *daf-2(e1370)* and *daf-16(mu86)* mutants (Fig. S2A and B), which model aging effects, with *daf-2(e1370)* mutants showing a slower aging rate and extended life span while *daf-16(mu86)* mutants age faster than the wild type and have a shortened life span.<sup>11</sup> The *daf-2(e1370); V1S+SV2* animals showed a reduced BiFC signal (Fig. 2A and B; Fig. S2D), a smaller number of inclusion bodies (Fig. 2C and D; Fig. S2E), less nerve degeneration (Fig. 2E and F; Fig. S2F and G) improved pumping behavior (Fig. 2G; Fig. S2H), and extended life span than the V1S+SV2 line (Fig. 2H; Fig. S2I). Conversely, in the *daf-16(mu86); V1S+SV2* animals, BiFC-positive inclusion bodies appeared much earlier than in the V1S+SV2 animals; as early as 2-d post the L4-stage (Fig. 2C and D; Fig. S2E). The BiFC signal itself was lower in the *daf-16(mu86); V1S+SV2* than in the V1S+SV2 (Fig. 2B; Fig. S2D), probably due to early and robust formation of inclusion bodies. The *daf-16(mu86); V1S+SV2* animals showed more severe nerve degeneration (Fig. 2E and F; Fig. S2F and G), more decreased pumping behavior (Fig. 2G; Fig. S2H), and shorter life span than the V1S+SV2 animals (Fig. 2H; Fig. S2I). Similar results were obtained in 3 independent lines for each genotype. These results indicate that genetic factors affecting aging processes might change the rate of cell-to-cell transmission of SNCA aggregates and the associated degenerative phenotypes in vivo.

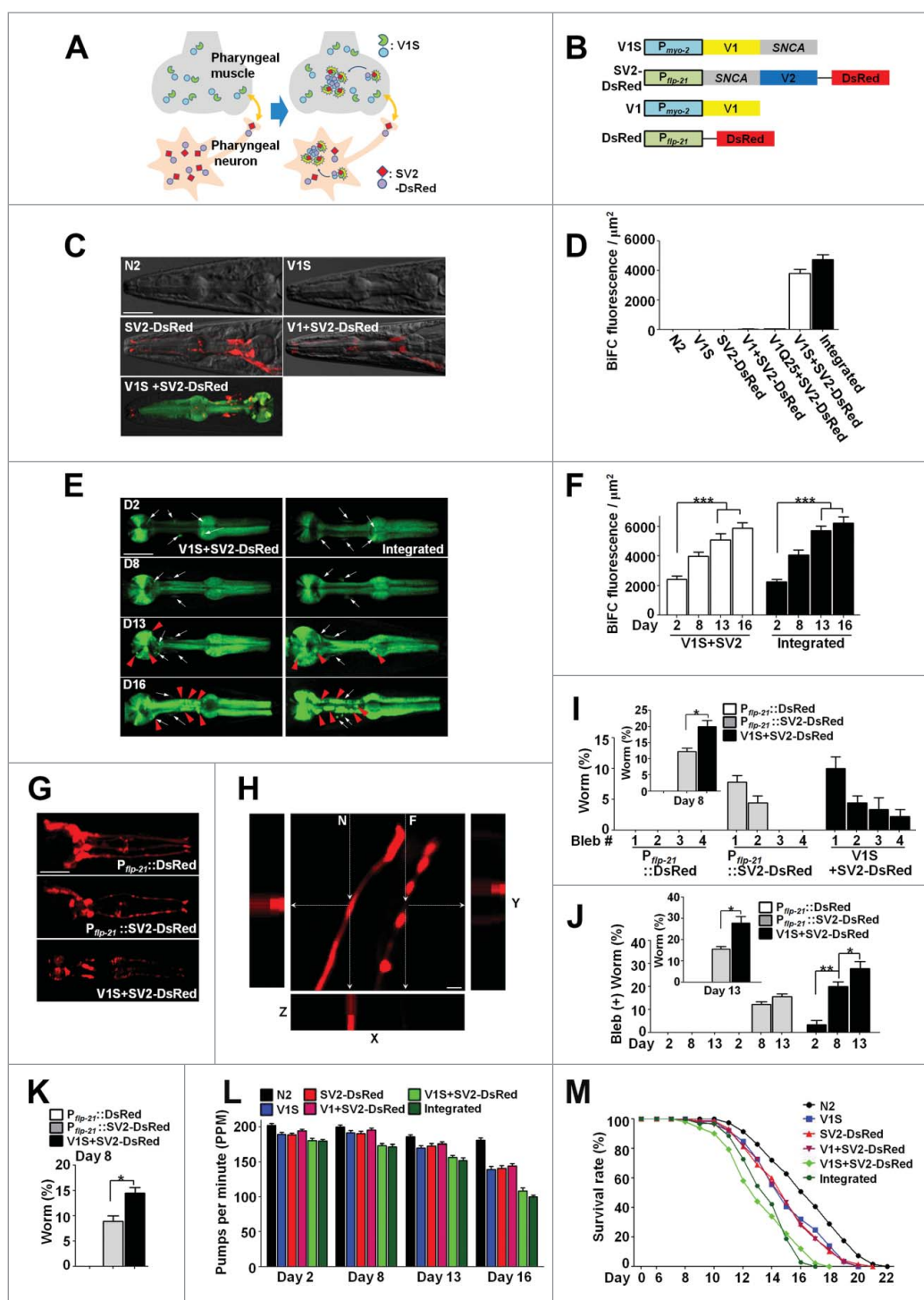


**Figure 1.** Generation and characterization of the *C. elegans* model for transmission of synucleinopathy. (A) Postulated events leading to the generation of BiFC fluorescence via cell-to-cell transmission of SNCA. (B) Transgenes used in *C. elegans*. DsRed is expressed as an independent translational unit, which is used to label neurons. (C) BiFC fluorescence in pharyngeal muscles and neurons. All pictures contain DIC and fluorescence images. The arrows indicate BiFC signals from neurons (see also Fig. S1E to H). Scale bars: 200  $\mu\text{m}$ . (D) Quantification of BiFC fluorescence in (C) and the V1S + SV2 double-transgenic integrated line. Twenty-five worms from each line were used. (E) Increase in BiFC fluorescence with aging. White arrows indicate the BiFC signals in neurons, and red arrowheads indicate inclusions in the pharynx. Scale bars: 200  $\mu\text{m}$ . (F) Quantification of BiFC fluorescence in (E) and the V1S+SV2 double transgenic integrated line. Twenty-five worms from each line were used; \*\*\*,  $P < 0.001$ . (G) Nerve processes expressing DsRed were analyzed for neurodegeneration. Scale bars: 200  $\mu\text{m}$ . (H) A 3-dimensional reconstruction of axonal processes from URA motor neuron containing DsRed fluorescence. N, normal axonal process; F, fragmented axonal process. "Fragmented" represent complete degeneration of nerves. Scale bars: 40  $\mu\text{m}$ . (I and J) Blebbing phenotype. Percentage of worms that have blebs at d 8 (I) and blebbing phenotype with aging (J). Thirty worms from each line were used,  $n = 3$ ; \*,  $P < 0.05$ ; \*\*,  $P < 0.01$ . (K) Fragmentation of axonal process at d 8. Thirty worms from each line were used,  $n = 3$ ; \*,  $P < 0.05$ . (L) Pharyngeal pumping rate with aging; Twenty-five worms from each line were used,  $P$  values are listed in Table S1. (M) Life-span analyses. One hundred fifty worms for each line were used,  $P$  values are listed in Table S2.

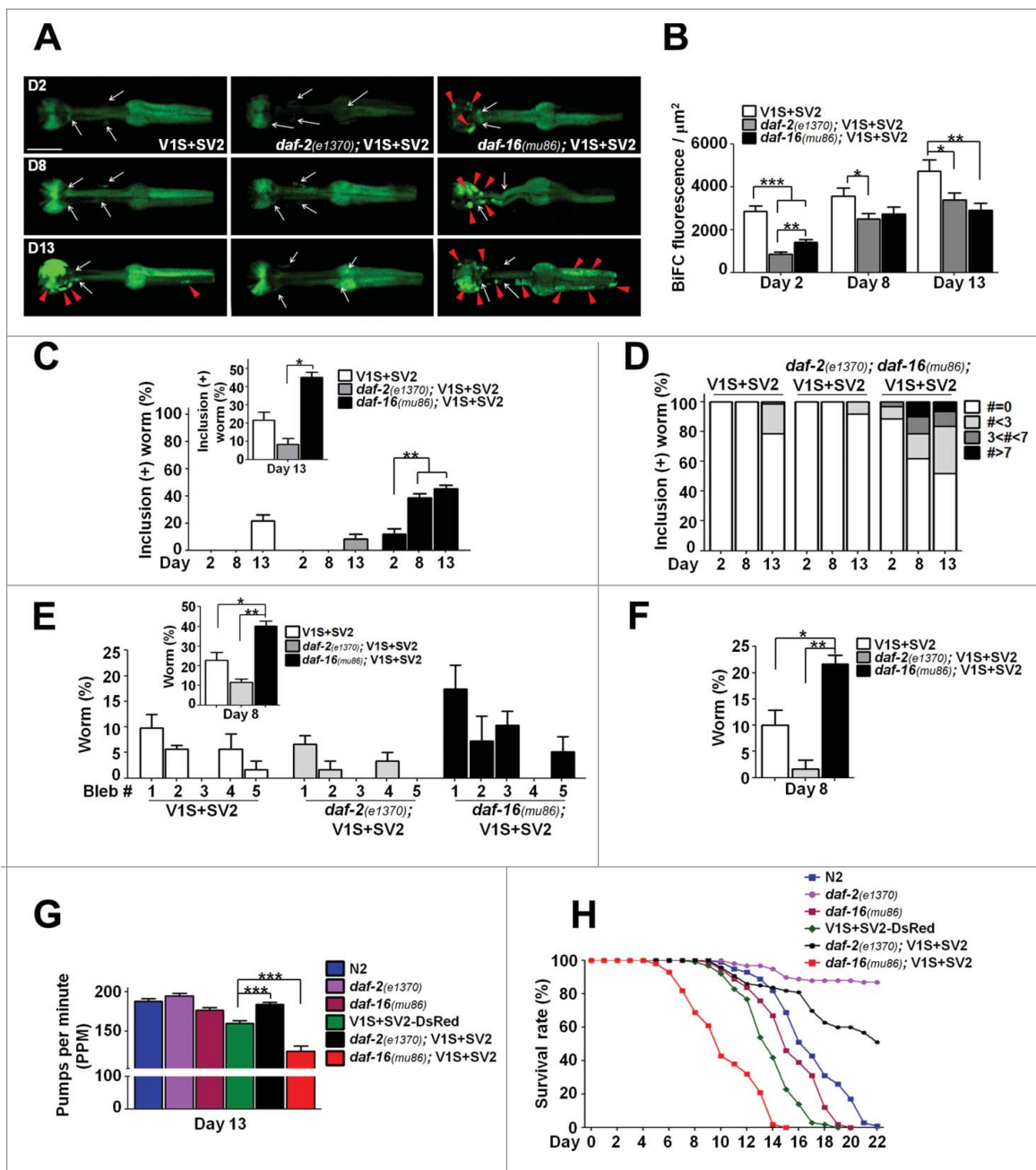


**Figure 2.** Effects of *daf-2*, *daf-16* mutants on cell-to-cell SNCA transmission. (A and B) BiFC fluorescence in the aging-related mutants, *daf-2(e1370)* and *daf-16(mu86)* (see also Fig. S2D). Scale bars: 200 µm (A). Twenty worms for each line were used,  $n = 3$ ; \*,  $P < 0.05$ ; \*\*,  $P < 0.01$ ; \*\*\*,  $P < 0.001$ . (C and D) Percentage of worms that have BiFC-positive inclusions with aging (see also Fig. S2E). Twenty worms for each line were used,  $n = 3$ ; \*,  $P < 0.05$ ; \*\*,  $P < 0.01$ . (E and F) Quantification of axonal bleb number (E) and nerve fragmentation (F) at d 8 (see also Fig. S2F and G). Twenty worms for each line were used,  $n = 3$ ; \*,  $P < 0.05$ ; \*\*,  $P < 0.01$ . (G) Pharyngeal pumping rates at d 13 (see also Fig. S2H). Twenty worms for each line were used,  $n = 3$ ; \*\*,  $P < 0.01$ . (H) Life-span analyses (see also Fig. S2I). Three hundred worms for each line were used,  $P$  values are listed in Table S2.

### Effects of pharmacological anti-aging treatment on transcellular SNCA transmission

We then sought to determine the effects of the anti-aging agent, *N*-acetylglucosamine (GlcNAc)<sup>12</sup> on aggregate transmission. When GlcNAc was administered to the V1S+SV2 and *daf-16(mu86); V1S+SV2* animals, both animals showed reduced formation of BiFC-positive inclusion bodies (Fig. 3A and B) and significantly alleviated phenotypes for nerve degeneration (Fig. 3C to F), pumping behavior (Fig. 3G), and life span (Fig. 3H). These results suggest that pharmacological anti-aging treatments can slow the progress of synucleinopathy.

### Changes in steady-state levels of polyubiquitinated proteins by anti-aging treatment

To confirm the microscopy data for changes in the levels of aggregates, we performed a dot blot analysis with an antibody specific to  $\beta$ -sheet-rich SNCA multimers (Syn-O2).<sup>13</sup> Consistent with the BiFC inclusion analysis, the dot blot analysis showed that  $\beta$ -sheet-rich SNCA aggregates were reduced by the *daf-2* mutation and by GlcNAc, whereas the *daf-16* mutation increased the aggregates (Fig. 4A and B).

Aging causes a progressive decline in protein homeostasis.<sup>12,14,15</sup> This led us to examine the steady-state levels of

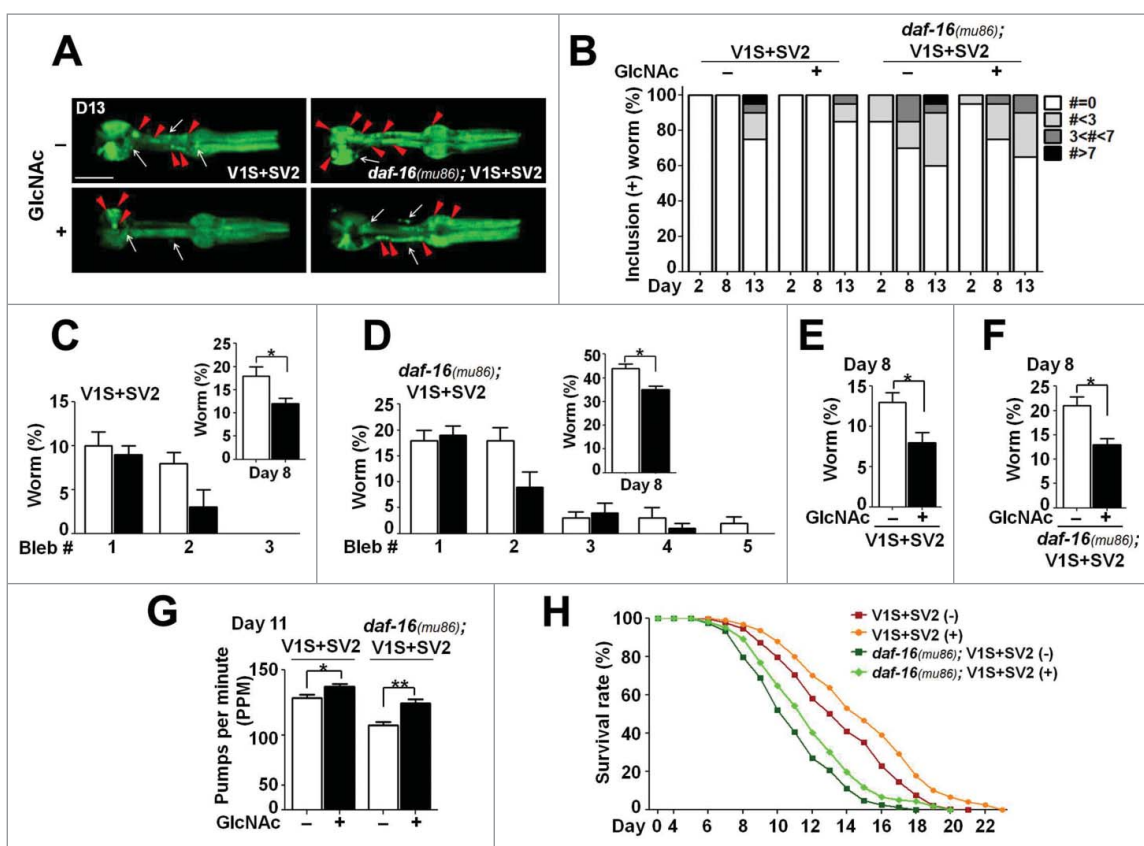


**Figure 3.** Effects of GlcNAc in transcellular SNCA transmission. (A) Changes in BiFC fluorescence with GlcNAc treatment at d 13. The white arrows indicate BiFC signals from neurons, and the red arrowheads indicate inclusions in pharynx. Scale bars: 200  $\mu$ m. (B) Worms with BiFC-positive inclusions were quantified. Thirty worms for each line were used. (C and D) Axonal bleb numbers in the V1S+SV2 (C) and *daf-16(mu86)*; V1S+SV2 animals (D) with GlcNAc treatment at d 8. Twenty worms for each line were used,  $n = 5$ ; \*,  $P < 0.05$ . (E and F) Nerve fragmentation in the V1S+SV2 (E) and *daf-16(mu86)*; V1S+SV2 (F) transgenic lines at d 8. Twenty worms for each line were used,  $n = 5$ ; \*,  $P < 0.05$ . (G) Pharyngeal pumping rates at d 11. Forty worms for each line were used; \*,  $P < 0.05$ ; \*\*,  $P < 0.01$ . (H) Life-span analyses with GlcNAc treatment. Five hundred worms for each line were used,  $P$  values are listed in Table S2.

polyubiquitinated proteins, which represent the activities of major protein degradation systems, such as the ubiquitin-proteasome system and autophagy. The levels of polyubiquitinated proteins were increased in the *daf-16* transgenic animals, while they were decreased in the *daf-2* transgenic animals (Fig. 4C to F). Similarly, the treatment of animals with GlcNAc decreased the levels of polyubiquitinated proteins (Fig. 4G to J). These results suggest that the effects of aging and anti-aging treatments on the propagation of synucleinopathy are mediated by the changes in the capacity of protein degradation systems.

### The endolysosomal pathway in SNCA transmission

Previous studies in cell models have shown that intercellular SNCA transmission is mediated by endocytosis, and the transferred proteins are delivered to lysosomes for degradation.<sup>16–19</sup> When V1S+SV2 was introduced into dynamin mutants, *dyn-1(ky51)*,<sup>20</sup> BiFC fluorescence was significantly reduced compared to that in the wild type (Fig. 5A and B). Reduction of the BiFC signal in the *dyn-1(ky51)* transgenic animals was greater at d 5 than at d 2, suggesting that the effect was cumulative. Our previous studies have shown that lysosomal function is important for clearing the “seeds” in the process of intercellular SNCA transmission, and lysosomal dysfunction resulted in an enhancement of aggregate transmission.<sup>17,19,21</sup> Consistent with these studies, when V1S+SV2 was introduced into the *asp-4*

(*ok2693*) and *asp-1(tm666)* mutants, carrying mutations in cathepsin genes,<sup>22</sup> BiFC fluorescence was significantly increased in both mutants, often in the form of inclusion bodies (Fig. 5C to E; Fig. S3D and E). These results suggest that lysosomal responses are crucial for protecting the animals from age-dependent aggregate propagation. Consistent with this interpretation, GlcNAc treatment increased the expression of lysosomal genes such as *lmp-1/LAMP1*, *sul-3/ARSB* and *asp-1/CTSD* (Fig. 4K and L). This was further validated by epistasis analysis, where *asp-4(ok2693)*; V1S+SV2 and *asp-1(tm666)*; V1S+SV2 worms were treated with GlcNAc. In contrast to the V1S+SV2 worms, aging-related phenotypes were not rescued by GlcNAc treatment in the *asp-1* and *asp-4* mutant transgenic animals (Fig. 5F to J). We also analyzed the expression of *sqst-1/p62*, a key component of the autophagic process, and its expression seemed to be upregulated, although the change failed to exhibit statistical significance (Fig. 4K and L).

### The effects of anti-aging treatments on aggregate transmission are associated with enhanced lysosomal function

To verify the role of lysosome in protection against aggregate propagation, we generated the *hlh-30* transgenic lines overexpressing the vector *hlh-30p::hlh-30*,<sup>14</sup> an ortholog of TFEB, the master control transcription factor for lysosome biogenesis,<sup>23</sup>

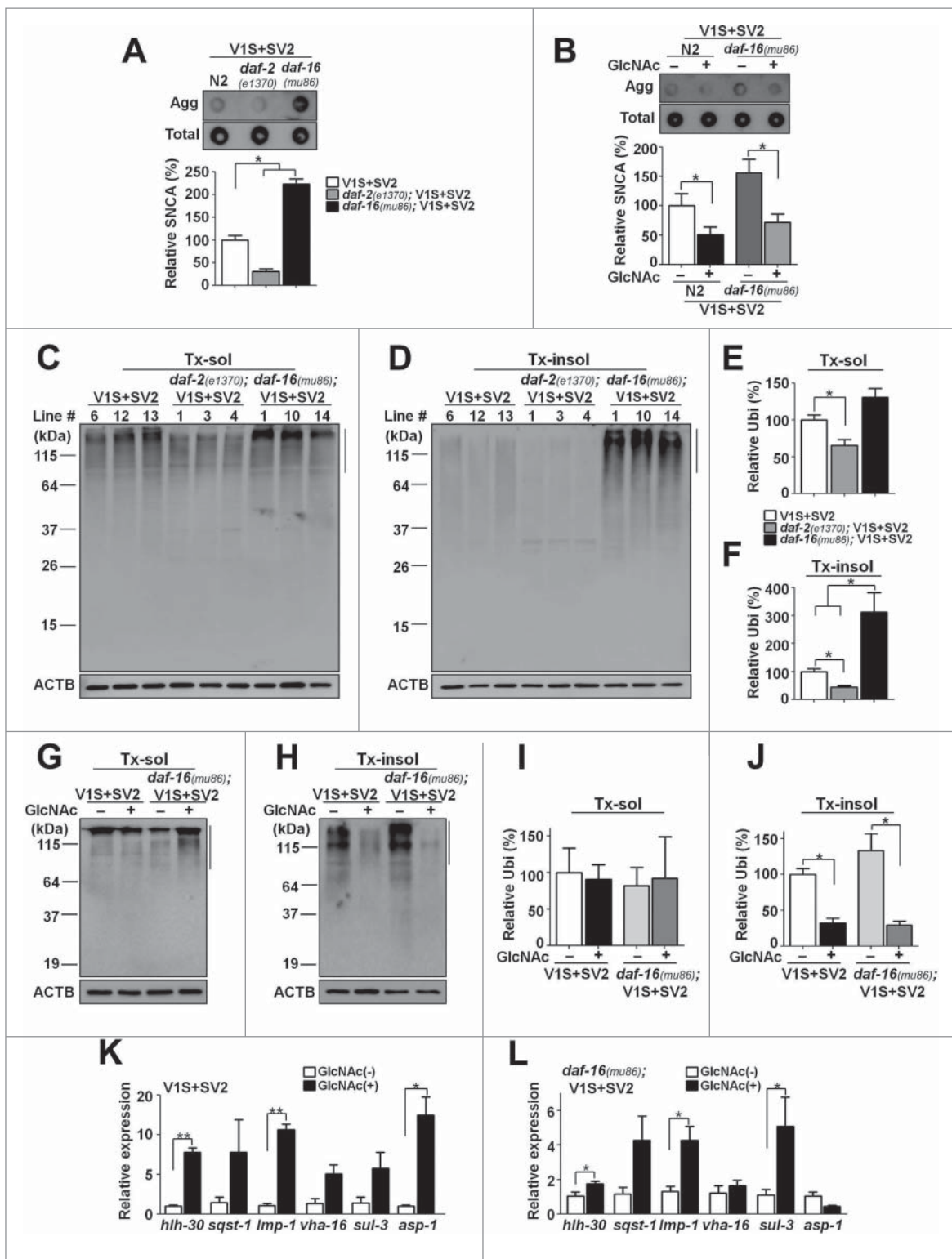


**Figure 4.** Changes in steady-state levels of polyubiquitinated proteins by anti-aging treatment. (A and B) Levels of SNCA aggregates (Syn-O2) in aging-related lines and with GlcNAc treatment. The data were normalized to total SNCA expression (274). Agg, SNCA aggregates; Total, total SNCA expression,  $n = 3$  (A),  $n = 5$  (B); \*,  $P < 0.05$ . (C and D) The levels of polyubiquitinated proteins in aging-related models. (E and F) Quantification of the levels in Tx-sol (E) and Tx-insol (F) fractions. The levels were highest in *daf-16(mu86); V1S+SV2* lines. Tx-sol, Triton-soluble; Tx-insol, Triton-insoluble,  $n = 3$ ; \*,  $P < 0.05$ . (G and H) The levels of polyubiquitinated proteins with GlcNAc treatment in aging-related models. (I and J) Quantification of the levels in Tx-sol (I) and Tx-insol (J) fractions.  $n = 5$ ; \*,  $P < 0.05$ . All the line on the right side of western images indicates the quantified size range in the blots. All the data were normalized to ACTB expression. (K and L) Expression levels of autophagy-related and lysosomal genes in the V1S+SV2 (K) and *daf-16(mu86); V1S+SV2* animals (L) with GlcNAc treatment measured by qPCR.  $n = 5$ ; \*,  $P < 0.05$ ; \*\*,  $P < 0.01$ .

into the *daf-16(mu86); V1S+SV2* transgenic animals (Fig. S4A). In addition to lysosomal and autophagic genes, downstream target genes for HLH-30/TFEB include genes

involved in metabolism, apoptosis, and signaling.<sup>24</sup> Expression of *hlh-30::hlh-30* in the *daf-16(mu86); V1S+SV2* animals increased the expression of lysosomal gene, *asp-1* as well as the

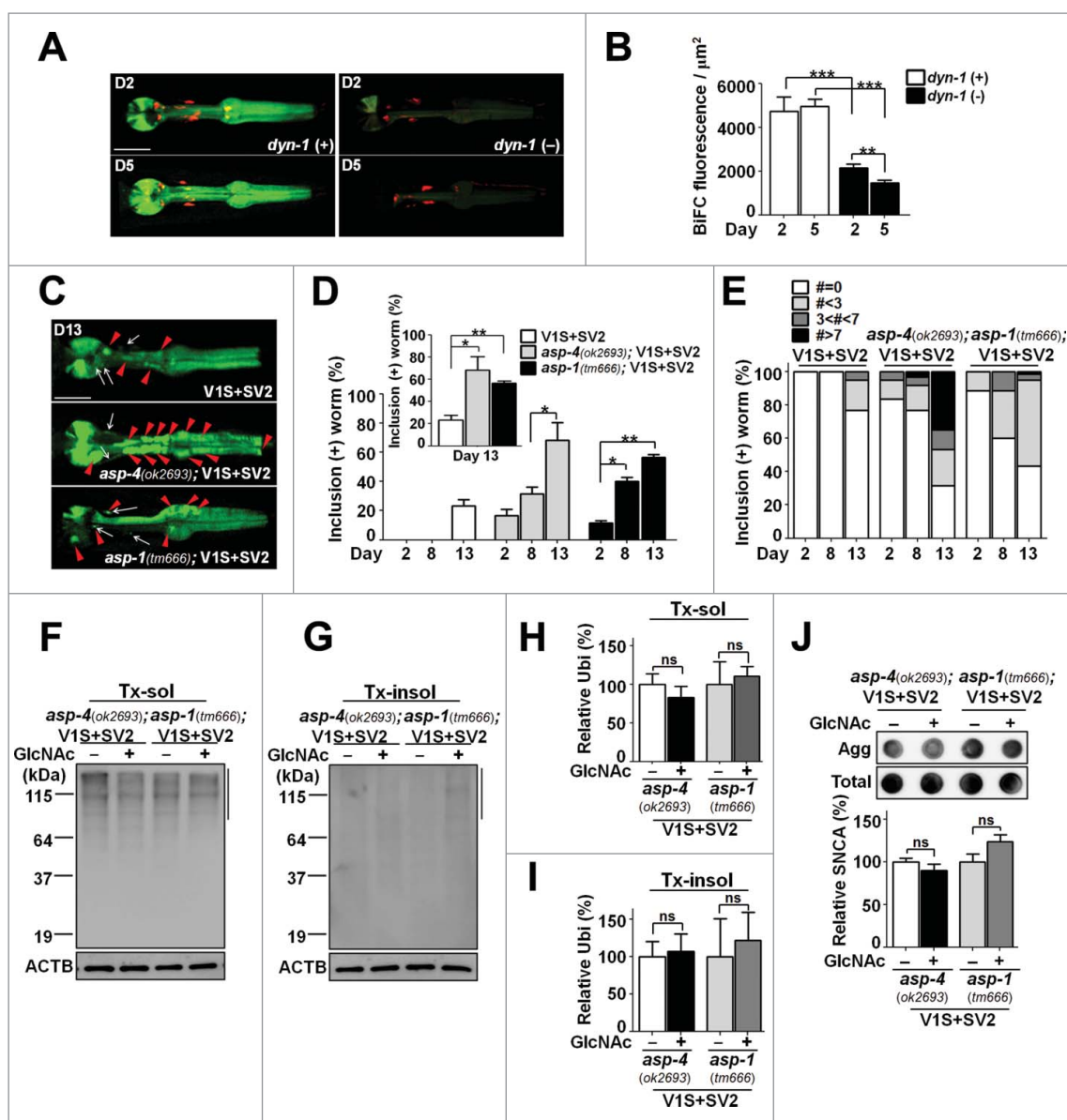


**Figure 5.** Involvement of the endolysosomal pathways in SNCA transmission. (A and B) BiFC fluorescence in wild-type and *dyn-1(ky51)* transgenic lines. Scale bars: 200  $\mu\text{m}$  (A). Twenty-four worms for each line were used; \*\*,  $P < 0.01$ ; \*\*\*,  $P < 0.001$ . (C to E) BiFC fluorescence and inclusion body formation in wild-type, *asp-4(ok2693)* and *asp-1(tm666)* mutant worms (see also Fig. S3D and E). Scale bars: 200  $\mu\text{m}$  (C). Twenty worms for each line were used,  $n = 3$ ; \*,  $P < 0.05$ ; \*\*,  $P < 0.01$ . (F to J) Epistasis analysis of *asp-4* and *asp-1* transgenic worms with GlcNAc treatment. (F and G) The levels of polyubiquitinated proteins with GlcNAc treatment. (H and I) Quantification of the levels in Tx-sol (H) and Tx-insol (I) fractions. (J) Levels of SNCA aggregates with GlcNAc treatment. The data were normalized to ACTB (F and G) and total SNCA expression (J),  $n = 3$ , ns: not significant.

gene involved in autophagy, *sqs-1* (Fig. 6A), and reduced and the steady-state levels of polyubiquitinated proteins (Fig. 6B to E), which indicate the restoration of protein degradation, and the formation of SNCA aggregates (Fig. 6F). The *hlh-30p::hlh-30* transgenic lines showed reduced BiFC signal (hence, reduced aggregate propagation), decreased nerve degeneration, increased pumping rates, and increased life span (Fig. 7A to H; Fig. S4B to D).

### Cell-autonomous aggregation vs. intercellular transmission

The results presented above do not differentiate between intercellular aggregate transmission and cell-autonomous aggregation. To address this issue, we have generated 4 transgenic lines

expressing V1S or SV2 alone in N2 and *daf-16(mu86)* mutant worms. Also 2 transgenic worms overexpressing the *hlh-30p::hlh-30* transgene with V1S or SV2 were generated. Expression levels were normalized with single-worm PCR and western analysis (in case of V1S lines) or DsRed fluorescence (in case of SV2 lines). Nerve degeneration, pumping behavior, and life span of the transgenic worms in mutant backgrounds were compared with the ones in normal genetic background. We did not find significant differences in the phenotypes (Fig. S5C to G), suggesting the genetic modification we investigated does not have a large impact on SNCA aggregation in the respective tissues (Fig. S5H).

We also treated the single-tissue expression lines carrying V1S or SV2 alone in N2 and *daf-16(mu86)* mutant worms with GlcNAc and compared the same battery of phenotypic assays

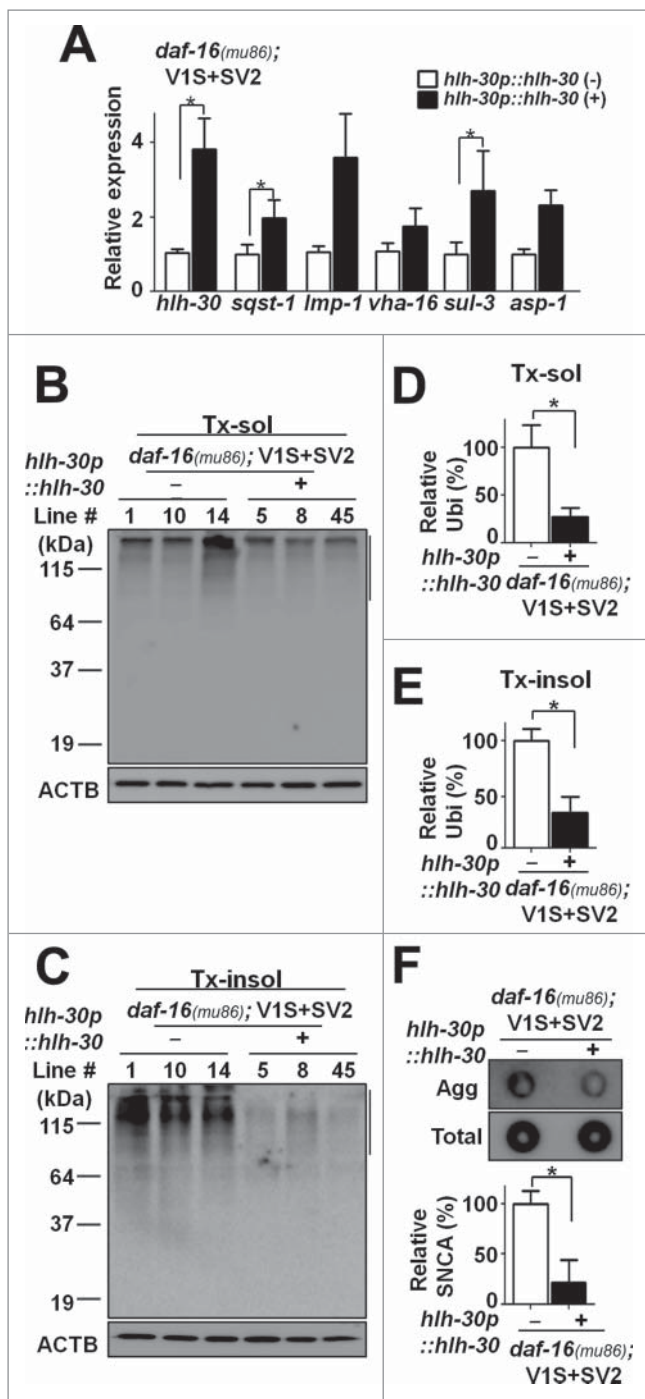


**Figure 6.** Restoration of lysosomal degradation function by transgenic expression of *hlh-30p::hlh-30*. (A) Expression levels of autophagy-related and lysosomal genes measured by qPCR.  $n = 3$ ;  $^*P < 0.05$ . (B and C) The levels of polyubiquitinated proteins in *daf-16(mu86); V1S+SV2* in the presence or absence of the *hlh-30p::hlh-30* transgene. (D and E) Quantification of the levels in Triton-soluble (D) and Triton-insoluble (E) fractions. The size ranges quantified are indicated by the line to the right in the blots. All the data were normalized with ACTB,  $n = 3$ ;  $^*P < 0.05$ . (F) Levels of SNCA aggregates in the *hlh-30p::hlh-30* transgenic lines. The data were normalized to total SNCA expression,  $n = 3$ ;  $^*P < 0.05$ .

with untreated animals. Unlike the transmission models, the single-tissue expression lines did not exhibit significant changes in pathogenic phenotypes upon treatment with GlcNAc (Fig. S6D to M). To examine the effects of GlcNAc on the expression levels of SNCA, we measured the levels of SNCA by dot blot (Fig. S6N and O). The data showed that the expression

levels were not changed by GlcNAc treatment. We also examined neuronal expression of *flp-21* promoter upon GlcNAc treatment by monitoring DsRed. Expression of DsRed was strictly confined in neuronal cells with or without GlcNAc treatment (Fig. S6P), indicating that the treatment does not change the cell-type specificity of the promoter.

Finally, we examined the detergent solubility of SNCA in the single (V1S or SV2) and double (V1S+SV2) transgenic worms with or without GlcNAc treatment. Triton X-100-insoluble to -soluble ratio was drastically increased in the double transgenics compared with the single transgenic, even though the expression level of each protein is supposedly the same (Fig. 8A to E; Fig. S8). This result implicates transcellular aggregate amplification between the pharyngeal muscle and the associated neurons. Dot blot with the aggregate-specific Syn-O2 antibody showed the similar results, confirming that the double transgenic produced much more aggregates than the sum of each single transgenic (Fig. 8F). Another important point here is that the single transgenic indeed produced SNCA aggregates. This confirms that cell-autonomous aggregation does occur, so transmission of the aggregates can be initiated.

In the detergent solubility experiment, the Triton-insoluble to -soluble ratio was not changed upon GlcNAc treatment in single transgenics, whereas the same treatment greatly reduced the ratio (Fig. 8C to E; Fig. S8), suggesting that the anti-aging treatment affected primarily the transmission process, rather than the de novo aggregation of each protein. Dot blot analysis with the Syn-O2 antibody showed largely the same results (Fig. 4B; Fig. S6N). These results suggest that the anti-aging and prolysosomal treatments used in the current study exert their effects on intercellular aggregate transmission.

## Discussion

We have developed a quantitative, real-time technique for the study of cell-to-cell transmission of SNCA in *C. elegans*. The model exhibits many key features of synucleinopathy, including the progressive accumulation of SNCA aggregates, nerve degeneration, behavioral deficits, and reduced life span. Both the genetic and pharmacological manipulations of animals have shown strong correlations among aging rates, transcellular SNCA transmission, and neurodegenerative phenotypes, and likewise, various manipulations associated with anti-aging effects can slow the progression of these events. Aging-dependent progression of synucleinopathy is accompanied by a decline in protein degradation. Anti-aging treatments can restore the systems mediating protein degradation. Furthermore, restoration of lysosomal function alleviated the propagation of aggregates and the accompanying neurodegeneration in these aging models.

BiFC is a widely used fluorescence technique that has been successfully applied to assess protein-protein interactions and protein dimerization and/or oligomerization in living cells.<sup>7</sup> The V1S-SV2 BiFC pair has been shown to fluoresce upon dimerization/oligomerization of SNCA when these proteins are coexpressed in mammalian cells.<sup>7</sup> In a previous study,<sup>17</sup> by generating neuroblastoma cell lines expressing either one of V1S and SV2, we have shown that cell-to-cell transfer of SNCA proteins and coaggregation of the transferred proteins with the



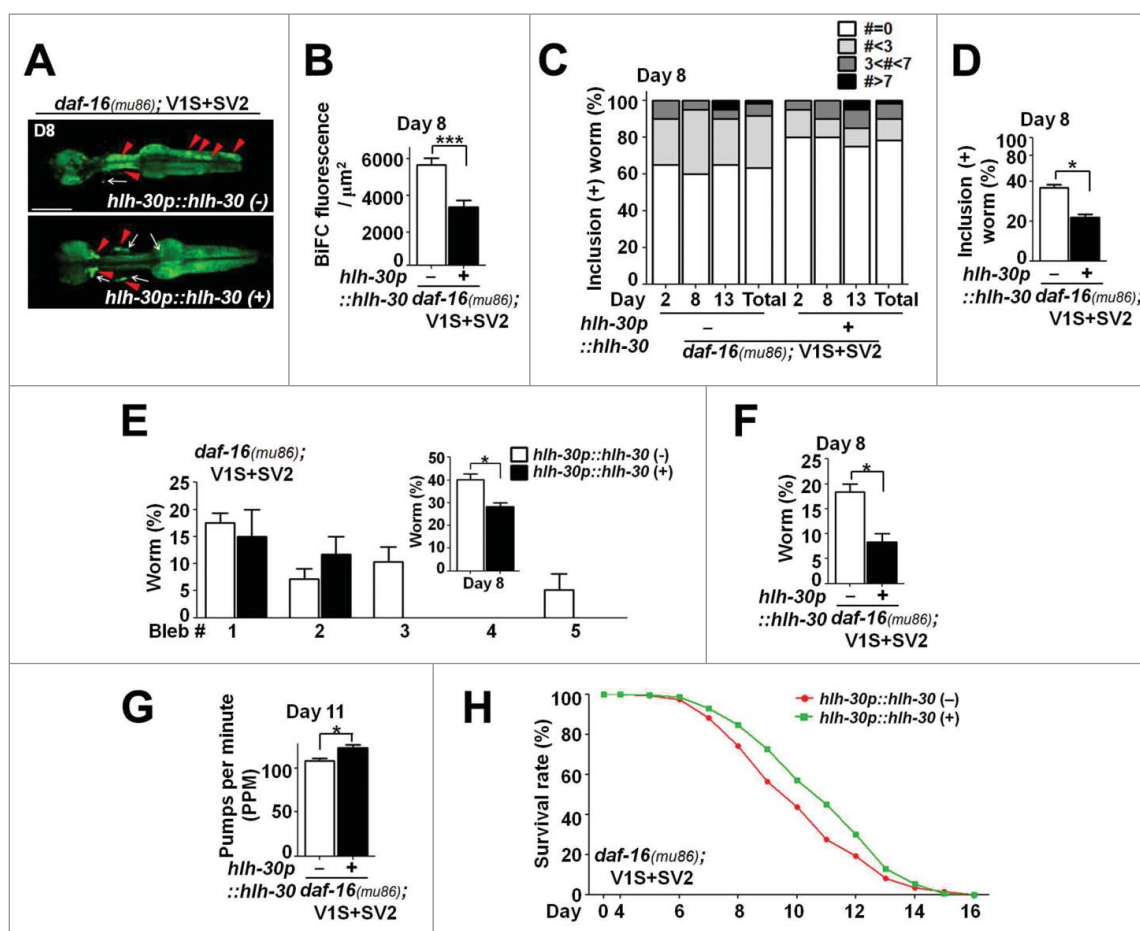


**Figure 7.** Reduced aggregate transmission with enhanced lysosomal function. (A and B) BiFC fluorescence in *daf-16(mu86); V1S+SV2* animals in the presence or absence of the *hlh-30p::hlh-30* transgene (see also Fig. S4B). Scale bars: 200  $\mu\text{m}$  (A). Twenty worms for each line were used,  $n = 3$ ; \*\*\*,  $P < 0.001$ . (C and D) BiFC-positive inclusions at d 8. Twenty worms for each line were used,  $n = 3$ ; \*,  $P < 0.05$ . (E) Axonal bleb numbers at d 8. Twenty worms for each line were used,  $n = 3$ ; \*,  $P < 0.05$ . (F) Nerve fragmentation at d 8. Twenty worms for each line were used,  $n = 3$ ; \*,  $P < 0.05$ . (G) Pharyngeal pumping rates at d 11 (see also Fig. S4C). Twenty worms for each line were used,  $n = 3$ ; \*\*,  $P < 0.01$ . (H) Life-span analyses (see also Fig. S4D). Three hundred worms for each line were used,  $P$  values are listed in Table S2.

endogenous SNCA can be visualized with BiFC fluorescence during coculture of these cells.

One of the important technical issues of the BiFC system is to verify the cell type-specific expression of each protein. Although quantitative analysis of SNCA transgenic expression in each cell type is not technically feasible, we have a series of data supporting the argument that SNCA is exclusively expressed only in the intended cell types. First, DsRed fluorescence is detected only in *flp-21* neurons, not in the pharyngeal muscle cells at all. Second, immunofluorescence staining of SNCA with a highly specific and sensitive antibody exhibited the expression of this protein specifically in the intended cell types. Third, expression of the same BiFC pair in the worms with the *dyn-1* mutation significantly reduced the BiFC fluorescence signal, indicating that generation of the BiFC fluorescence requires endocytosis. This suggests that the BiFC signal did not come from coexpression of the BiFC pair in the same cell types, but derived from intercellular transmission of the proteins.

Although the correlations between SNCA aggregate transmission and the degenerative phenotypes presented in this study are robust and consistent, we should stress that this study does not provide definitive evidence for the cause-consequence relationship between the aggregate transmission and neurodegeneration. Thus

far, no animal model studies have clearly addressed the cause-consequence issue. The *C. elegans* model we generated in this study will be a valuable tool in addressing this issue. One of the important purposes of developing the BiFC system is to identify genetic and small molecule modifiers that regulate the transmission. By identifying the modifiers, one should be able to regulate the rate and extent of the intercellular transmission, thereby solving the cause-consequence problem. The fact that the transcellular coaggregation of SNCA was greatly modulated by mutations in such genes as *dyn-1*, *asp-4*, *asp-1*, *daf-2*, and *daf-16*, indicates that this system is amenable to modulation by genetic factors and this validates the system for identification of novel genetic modulators. In addition, the distinctive structure of the pharynx in *C. elegans* would allow for the convenient identification of changes in transmission of synucleinopathy in large-scale screening for genetic and small-molecule modifiers.

Effects of aging processes on “transmission,” rather than the aggregation itself, is the key subject of the paper. Now, we would like to make it clear that we are not trying to argue that aging and lysosomal dysfunction only affect the transmission of aggregates without affecting cell-autonomous aggregation itself. Our BiFC system is an excellent system to quantify the transmission event, but not designed to monitor the cell-autonomous aggregation. Previous studies,<sup>25–27</sup> including our own,<sup>28</sup>

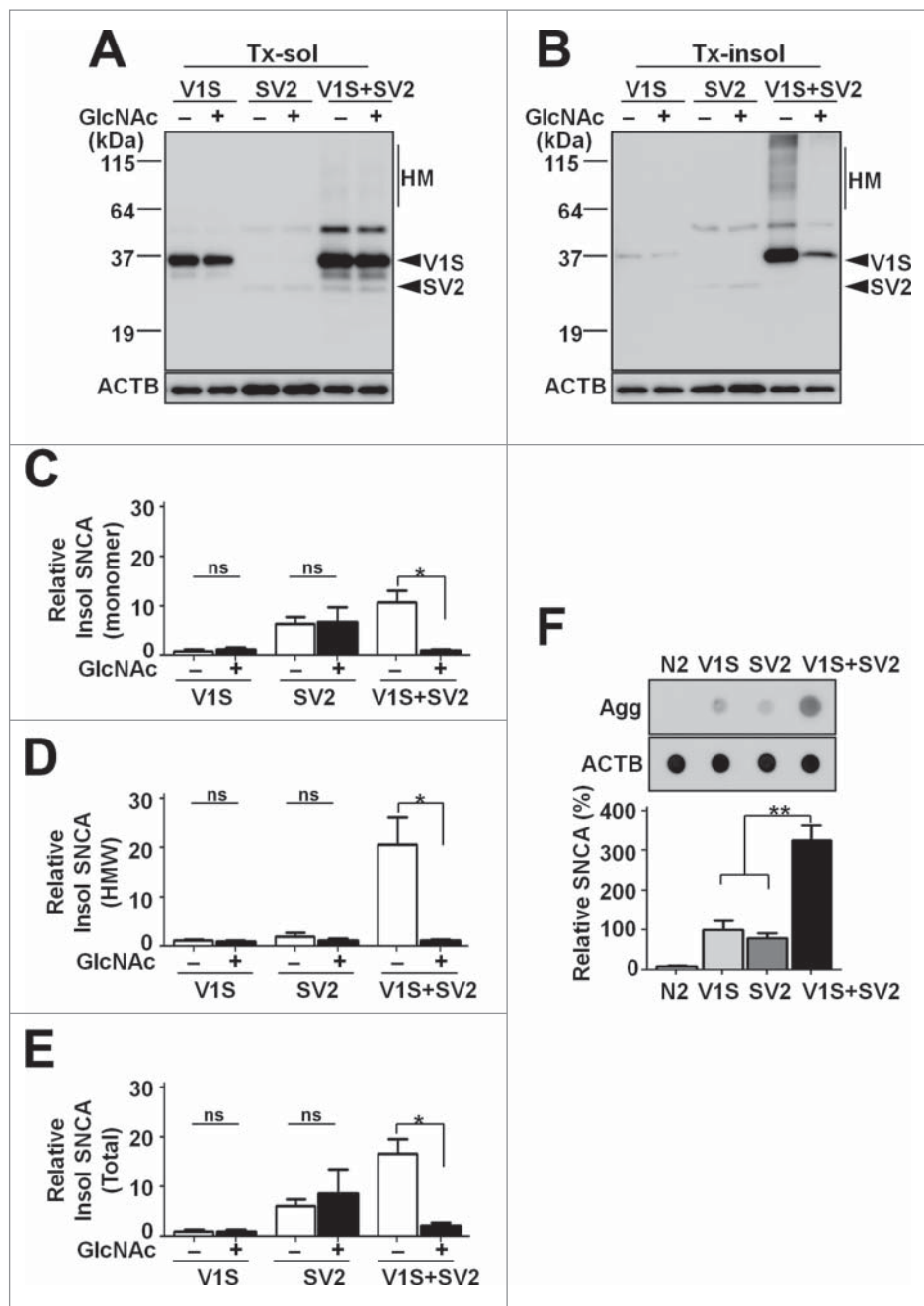


**Figure 8.** Alterations in accumulation of SNCA aggregates by transcellular transmission. (A to E) Western blot analysis in transgenic models with GlcNAc treatment (see also Fig. S8). (A and B) SNCA in Tx-sol (A) and Tx-insol (B) fractions. HM, high molecular weight SNCA. (C to E) Quantification of the levels of accumulated SNCA aggregates in monomeric size (C), high molecular weight (D) and total SNCA (E). The Tx-insol to Tx-sol ratio was significantly increased in double-transgenic lines,  $n = 5$ ;  $*$ ,  $P < 0.05$ ; ns, not significant. (F) Levels of SNCA aggregates in single- and double-transgenic lines. The data were normalized to total ACTB expression,  $n = 5$ ;  $**$ ,  $P < 0.01$ .

address the effects of lysosomal dysfunction in clearance of cell-autonomous SNCA aggregation. However, we would also like to point out that there is no definitive proof that these studies have observed only the cell-autonomous aggregation with excluding the effects of transcellular aggregate transmission and amplification. We would also like to emphasize that aggregation initiation is an absolute requirement for aggregate transmission. In fact, we show that the basal level cell-autonomous aggregation occurs spontaneously even in single transgenic animals (Fig. 8F).

The anti-aging effects of GlcNAc had been described to be DAF-16-independent.<sup>12</sup> This indicates that GlcNAc rescues the

*daf-16* phenotype not by directly affecting the DAF-16 pathway, but by acting through independent aging pathways. The data we present suggest that SNCA transmission is not under control of a specific aging pathway, but is rather regulated by the general aging.

Our current study provides a basis for considering the use of general anti-aging approaches as therapeutic strategies for stopping or slowing the progression of PD and related synucleinopathies. In addition, enhancers of lysosomal function can be considered as candidates for therapies aiming to stop or delay the progression of these diseases. The same approach could in theory be applied to other age-related neurodegenerative

diseases, many of which are thought to progress through the propagation of specific protein aggregates. Assuming that the propagation of different protein aggregates shares the same basic principle, we cautiously speculate that anti-aging and pro-lysosome strategies could be developed into a general therapy for stopping the progression of many neurodegenerative diseases. This hypothesis can be addressed by applying the BiFC-based animal model to other transmission models involving MAPT, polyglutamine proteins, and TARDBP.<sup>1</sup>

## Materials and methods

### Strains and culturing of nematodes

All strains were handled using standard procedures and grown, on nematode growth medium (NGM) plates containing a lawn of *Escherichia coli* (*E. coli*) strain OP50 at 20°C.<sup>29</sup> Wild-type Bristol N2 and the mutant strains *unc-119(ed3)*, *dyn-1(ky51)*, and *asp-4(ok2693)* were obtained from the *Caenorhabditis* Genetics Center (CGC; University of Minnesota, St. Paul, MN, USA). The mutant strain *asp-1(tm666)* was provided by *C. elegans* National BioResource Project (NBRP; Tokyo Women's Medical University School of Medicine, Tokyo, Japan). The mutant strains *daf-2(e1370)* and *daf-16(mu86)* were generous gifts from Professor Kyuhyung Kim (DGIST, Daegu, Korea).

### Plasmids construction for *C. elegans*

V1S and SV2 template plasmids were generous gifts from Dr. Pamela McLean (Massachusetts General Hospital, Boston, MA, USA).

#### One) P<sub>myo-2</sub>::EGFP

The *myo-2* promoter (P<sub>myo-2</sub>) was PCR-amplified from genomic DNA obtained from wild-type N2 worms. A sense primer containing a *Hind*III site, 5'-GACAAGCTTGGGGTTTTGTGCTGTG-GACGTT-3' and an antisense primer containing a *Bam*HI site, 5'-GACGGATCCTTCTGTGTCTGACGATCGAGG-3' were used. P<sub>myo-2</sub>::EGFP was generated by inserting the PCR product into the *Hind*III and *Bam*HI sites of the pFX\_EGFP vector.<sup>30</sup>

#### Two) P<sub>myo-2</sub>::SNCA(Myc)

A sense primer containing a *Sal*I site, 5'-AGCGTCGACGC-CACCATGGATGTATTCATGAAAGGAC-3' and an antisense primer containing myc tag sequence and *Bgl*II site, 5'-AGCAGATCTACAGATCCTCTTCAGAGATGAGTTTCTGCTCG-GCTTCAGGTTTCGTAGTCTTG-3' were used to amplify the MYC-tagged human SNCA obtained from pcDNA3.1 MycHis-SNCA vector.<sup>28</sup> The EGFP fragment of P<sub>myo-2</sub>::EGFP was replaced by the PCR-amplified Myc tagged human SNCA fragment to construct P<sub>myo-2</sub>::SNCA(Myc).

#### Three) P<sub>myo-2</sub>::V1S

A sense primer containing a *Sal*I site, 5'-AGCGTCGACGC-CACCATGGTGTAGCAAGGCCGAGG-3' and an antisense primer containing a *Bgl*II site, 5'-AGCAGATCTTTAGGCTT-CAGGTTTCGTAGTC-3' were used to amplify V1S. In addition, the EGFP fragment of P<sub>myo-2</sub>::EGFP was replaced by the PCR-amplified V1S fragment to construct P<sub>myo-2</sub>::V1S.

#### Four) P<sub>myo-2</sub>::V1Q25

A sense primer containing a *cl*aI site, 5'-TAAGCAATCGA-TATGGCGACCCTGGAAAAGCTG-3' and an antisense primer

containing a *cl*aI site, 5'-TGCTTAATCGATAGGTCGGTGCA-GAGGCTCCTC-3' were used to amplify Q25. Then, the human SNCA fragment of P<sub>myo-2</sub>::V1S was replaced by the PCR-amplified Q25 fragment to construct P<sub>myo-2</sub>::V1Q25.

#### Four) P<sub>flp-21</sub>::SV2

The EGFP fragment of pFX\_EGFP was replaced by the PCR-amplified SV2 fragment to make an SV2 vector. The sense primer containing a *Spe*I site, 5'-AGCACTAGTGCCACCATGGATG-TATTCATGAAAGG-3' and an antisense primer containing a *Bgl*II site, 5'-AGCAGATCTTACTTGTACAGCTCGTCCATGC-CG-3' were used.

The *flp-21* promoter (P<sub>flp-21</sub>) was PCR-amplified from N2 genomic DNA and subcloned into *Kpn*I and *Sal*I sites of the SV2 vector to generate P<sub>flp-21</sub>::SV2. A sense primer containing a *Kpn*I site, 5'-AGCGGTACCAACTAGGTCCAGTGACCGAAAG-3' and an antisense primer containing a *Sal*I site, 5'-AGCGTCGACGCCAC-CATGGATGTATTCATGAAAGGAC-3' were used to amplify the *flp-21* promoter.

#### Five) P<sub>flp-21</sub>::SV2-ICR-DsRed

To make an SV2 vector coexpressing DsRed as a pharyngeal neuronal marker, P<sub>flp-21</sub> was subcloned into the *Kpn*I and *Sal*I sites of the pFX\_DsRedxT vector<sup>30</sup> and named P<sub>flp-21</sub>::DsRed. Coexpression of SV2 and DsRed under the *flp-21* promoter was achieved by placing an intercistronic region (ICR) between SV2 and DsRed, which was PCR-amplified from N2.<sup>31</sup> The SV2 fragment was fused with the ICR region by fusion PCR<sup>32</sup> and subcloned into the P<sub>flp-21</sub>::DsRed to construct P<sub>flp-21</sub>::SV2-ICR-DsRed. A sense primer containing a *Sal*I site, 5'-AGCGTC-GACGCCACCATGGATGTATTCATGAAAGGAC-3' and an antisense primer containing an overlapping region with an ICR, 5'-CGATCATTTTGGAGATTACTTGTACAGCTTGTCC-3' was used in the PCR reaction for SV2. The ICR region was amplified with a sense primer containing an overlapping region with SV2, 5'-GGACGAGCTGTACAAGTAATCTCCAAAAT-CATCG-3' and an antisense primer containing a *Spe*I site 5'-AGCACTAGTTACCCTGTAATAATATATTAAC-3'.

### Establishment of BiFC transgenic worms

P<sub>myo-2</sub>::V1S and P<sub>flp-21</sub>::SV2-ICR-DsRed plasmids were coinjected into the gonads of late L4-stage N2 worms with a selection marker, pRF4 which expresses a mutant collagen gene, *rol-6(su1006)*,<sup>33</sup> to make a double-transgenic line expressing the BiFC pair. As a negative control for BiFC, P<sub>myo-2</sub>::V1S alone was injected into N2 worms with pRF4, and P<sub>flp-21</sub>::SV2-ICR-DsRed alone was injected into *unc-119(ed3)* mutant worms with a selection marker, pCFJ151, which expresses *unc-119(+)* gene.<sup>34</sup> The plasmid P<sub>myo-2</sub>::V1 was generated to express the BiFC partial sequence only by introducing the stop codon right before the SNCA coding sequence in P<sub>myo-2</sub>::V1S using a Quik-Change Site-Directed Mutagenesis Kit (Stratagene, 200521). P<sub>myo-2</sub>::V1 and P<sub>flp-21</sub>::SV2-ICR-DsRed plasmids were then coinjected into N2 with pRF4. The plasmid P<sub>myo-2</sub>::V1Q25 was generated to express the huntingtin exon 1 with a 25 glutamine stretch by replacing SNCA with the Q25 fragment in P<sub>myo-2</sub>::V1S. P<sub>myo-2</sub>::V1Q25 and P<sub>flp-21</sub>::SV2-ICR-DsRed plasmids were then coinjected into N2 with pRF4. In addition, P<sub>flp-21</sub>::DsRed was injected into N2 with pRF4 as a control for the effects of general protein overexpression in neurons. For chromosomal

integration of the introduced plasmids, injected lines were exposed to UV irradiation. After UV irradiation, each integrated line was out-crossed 4 times with N2. Double transgenic lines carrying  $P_{myo-2}::V1S$  and  $P_{flp-21}::SV2$ -ICR-DsRed were generated by mating an integrated  $P_{myo-2}::V1S$  line with an integrated  $P_{flp-21}::SV2$ -ICR-DsRed line. All of these transgenic worms showed a roller phenotype and expression of DsRed fluorescence in the pharyngeal neurons.

### Generation of untagged SNCA models

$P_{myo-2}::SNCA$  and  $P_{flp-21}::SNCA$  plasmids were designed to express SNCA only by introducing stop codon right after the SNCA coding sequence by using a QuikChange Site-Directed Mutagenesis Kit. As a negative control,  $P_{myo-2}::SNCA$  alone was injected into N2 worms with pRF4.  $P_{myo-2}::SNCA$  and  $P_{flp-21}::SNCA$  plasmids were coinjected into the gonads of late L4-stage N2 worms with pRF4. All of these worms showed a roller phenotype and 3 representative lines of each genotype were used for experiments.

### Generation of aging-related BiFC models

$P_{myo-2}::V1S$  and  $P_{flp-21}::SV2$ -ICR-DsRed plasmids were coinjected into the gonads of late L4-stage *daf-2(e1370)* and *daf-16(mu86)* mutant worms with the pRF4. As a control for aging-related BiFC models,  $P_{myo-2}::V1S$  or  $P_{flp-21}::SV2$ -ICR-DsRed alone was injected into the gonads of late L4-stage of N2 and *daf-16(mu86)* mutant worms with pRF4. After several transgenic lines containing the introduced plasmids were obtained, 3 representative lines in each mutant background were used for experiments.

### Generation of *hlh-30p::hlh-30* transgenic lines

A plasmid expressing *hlh-30p::hlh-30::gfp* was a generous gift from Dr. Malene Hansen (Sanford-Burnham Medical Research Institute, CA, USA). The plasmid *hlh-30p::hlh-30* was designed to introduce stop codon before the GFP coding sequence using a QuikChange Site-Directed Mutagenesis Kit to inhibit GFP expression. As a control, each  $P_{myo-2}::V1S$  or  $P_{flp-21}::SV2$ -ICR-DsRed and *hlh-30p::hlh-30* were coinjected into the gonads of late L4-stage N2 worms with pRF4. The plasmids expressing  $P_{myo-2}::V1S$ ,  $P_{flp-21}::SV2$ -ICR-DsRed and *hlh-30p::hlh-30* were coinjected into the gonads of late L4-stage *daf-16(mu86)* mutant worms with pRF4. To analyze lysosomal dysfunction, *asp-4(ok2693)* and *asp-1(tm666)* mutant worms, in which the lysosomal enzyme cathepsin gene is inactivated, were used.  $P_{myo-2}::V1S$  and  $P_{flp-21}::SV2$ -ICR-DsRed plasmids were coinjected into the gonads of late L4-stage mutant worms with pRF4. After transgenic lines containing the introduced plasmids were obtained, 3 representative lines of each genotype were used for experiments.

### Immunofluorescence microscopy

For immunofluorescence staining of worms, wild-type N2 and transgenic worms were collected, washed with M9 buffer (22 mM  $KH_2PO_4$ , 22 mM  $Na_2HPO_4$ , 85 mM NaCl, 1 mM

$MgSO_4$ ), and then pre-fixed with 4% paraformaldehyde in MRWB (80 mM KCl, 20 mM NaCl, 10 mM EGTA, 5 mM spermidine [Sigma-Aldrich, S0266], 50% methanol). To reduce cuticle layer rigidity for penetrance, the worms were subjected to several freeze/thaw cycles using liquid nitrogen, and incubated with agitation at 4°C for 2 h. Because reduction and oxidation steps increase the permeability of the worm, the worms were washed with Tris-Triton buffer (100 mM Tris-HCl, pH 7.4, 1% Triton X-100 [Bio-Rad laboratories Inc., 161-0407], 1 mM EDTA), and incubated with 1%  $\beta$ -mercaptoethanol (Sigma-Aldrich, M7522) in Tris-Triton buffer at room temperature (RT) for 2 h. Subsequently, the worms were incubated in collagenase solution (100 unit of collagenase type IV [Worthington Biochemical Co., LS004188] in 100 mM Tris-HCl, pH 7.4, 1 mM  $CaCl_2$ , 0.1% Triton X-100) with rotation for 4 h at RT. Then the worms were incubated in Tris-Triton buffer supplemented with 0.3%  $H_2O_2$  (Sigma-Aldrich, H1009) for 15 min at RT. After incubation in blocking buffer (0.1% bovine serum albumin [BSA; Sigma-Aldrich, A7906], 0.5% Triton X-100, 1 mM EDTA in phosphate-buffered saline [PBS; GenDEPOT, CAP08-050]), the worms were incubated with monoclonal antibody 274 mAb<sup>10</sup> overnight at 4°C in primary antibody solution (1% BSA, 0.5% Triton X-100, 1 mM EDTA in PBS). The following day, the worms were washed with blocking buffer and incubated with rhodamine red X-conjugated goat anti-mouse IgG (1:100; Jackson ImmunoResearch Laboratories, 115-295-166) for 2 h. The worms were then washed with blocking buffer and mounted in Antifade reagent (Invitrogen, P36930). Samples were analyzed using an Olympus FV1000 confocal laser-scanning microscope (Olympus, Tokyo, Japan).

### Fluorescence microscopy of live worms

Worms were immobilized with 10 mM sodium azide in M9 buffer, and covered with a coverslip. Images of the worms were acquired using Olympus FV1000 confocal laser scanning microscopy.

### Western blotting

Adult worms were washed with M9 buffer and subsequently with PBS containing 1% Triton X-100. The worm pellet was sonicated in PBS containing 1% Triton X-100, 1% (vol/vol) protease inhibitor cocktail (Sigma-Aldrich, P8340) and centrifuged to obtain the Triton-soluble (supernatant) and -insoluble (pellet) fractions. Protein concentration was measured using the BCA protein assay (Pierce Biotechnology, 23223 and 23224). Protein samples (3  $\mu$ g for SNCA expression test, 50  $\mu$ g to detect polyubiquitin proteins, and 20  $\mu$ g (V1S, V1S+SV2 lines) and 40  $\mu$ g (SV2 lines) for differential solubility of SNCA) were loaded onto 12% SDS-PAGE gels. The primary antibodies used for western blotting were monoclonal anti-SNCA antibody, 274 mAb (1:1,500) and Syn-1 (1:1,500; BD BioScience, 610787), and anti-ubiquitin antibody (1:3,000; Abcam, ab7254). Chemiluminescence detection was performed using the LAS-3000 luminescence image analyzer (Fujifilm, Tokyo, Japan) and Amersham imager 600 (Ge Healthcare Life Sciences, Marlborough, MA, USA), and Multi Gauge (v3.0) software (Fujifilm, Tokyo, Japan).

### Dot blotting

Adult worms of each strain were washed with M9 buffer and subsequently with PBS containing 1% Triton X-100. The worm pellet was sonicated in PBS containing 1% Triton X-100 and 1% (vol/vol) protease inhibitor cocktail. Protein samples (500 ng) were loaded onto nitrocellulose membranes, which were then dried and incubated in blocking solution. The primary antibodies used for dot blotting were the monoclonal anti-SNCA antibodies 274 mAb and Syn-O2,<sup>13</sup> the latter of which is specific for SNCA aggregates. Chemiluminescence detection was performed using the LAS-3000 luminescence image analyzer and Amersham imager 600, and Multi Gauge (v3.0) software.

### Anti-aging agent treatment

*N*-acetylglucosamine (GlcNAc) (Sigma-Aldrich, A8625) was dissolved in distilled water to 1 M as stock solution. The stock solution was diluted with LB liquid medium (Sigma-Aldrich, L3022). The L4-stage worms of each transgenic line were transferred to NGM plates containing a final concentration of 10 mM GlcNAc.

### Single-worm PCR

A gravid single worm from each line was lysed in lysis buffer (50 mM KCl, 10 mM Tris-HCl, pH 8.3, 2.5 mM MgCl<sub>2</sub>, 0.45% NP-40 [IGEPAL; Sigma-Aldrich, I3021], 0.45% Tween 20 [Sigma-Aldrich, P1379]) with 0.1 mg/ml proteinase K (Sigma-Aldrich, P4850). The single worm in the buffer was subjected to several freeze-thaw cycles using liquid nitrogen, incubated at 65°C for 1 h to release genomic DNA, and then heated at 95°C for 15 min to inactivate proteinase K. Single-worm PCR analysis was performed using Ex Taq™ polymerase (Takara Biotechnology, RR001A) in Bio-Rad MyCycler PCR Thermal Cycler system (Bio-Rad Laboratories Inc., Hercules, CA, USA).

### PCR-restriction fragment length polymorphism genotyping

Gravid 5 worms from each line were lysed in the lysis buffer with 0.1 mg/ml proteinase K. Worms in the buffer were subjected to several freeze-thaw cycles using liquid nitrogen, incubated at 65°C for 1 h to release genomic DNA, and then heated at 95°C for 15 min to inactivate proteinase K. After performing PCR, the PCR products were digested with the *Nco*I enzyme (New England Biolabs Inc., R3193S), at 37°C overnight and electrophoresed to detect restriction fragment length polymorphism.

### Quantitative PCR (qPCR)

Adult transgenic worms were collected, and washed in M9 buffer. The worms in the buffer were sonicated and the samples were subjected to several freeze-thaw cycles using liquid nitrogen. RNA was extracted with Trizol Reagent (Invitrogen, 15596-026) and purified using the RNeasy mini kit (Qiagen, 74106). Each cDNA was synthesized from 500 ng of total RNA using the iScript cDNA synthesis kit (Bio-Rad Laboratories

Inc., 170-8891). For real-time PCR, target genes and specific primers were mixed with SYBR Premix Ex Taq II (Takara Biotechnology, RR081A) in 96-well plates. Specific primers previously designed by other group were used.<sup>14</sup> The DNA products were analyzed using the 7500 Real-Time PCR system (Applied Biosystems, Foster City, CA, USA). Relative mRNA levels of target genes were normalized to *act-1*.

### Heat-shock treatment of the *dyn-1* mutant

The double-transgenic worms (*P<sub>myo-2</sub>::V1S* + *P<sub>flp-21</sub>::SV2-ICR-DsRed*) were mated with *dyn-1(ky51)* mutant worms.<sup>20</sup> Adult mother worms of the double-transgenic line, with or without the *dyn-1(ky51)* mutation, were cultured on NGM plates containing *E. coli* OP50 for 4 h at 20°C to lay eggs, and were then removed. Synchronized progeny worms of each strain at the L4-stage were cultured at 30°C for observation.

### Pharyngeal pumping analysis

Pharyngeal pumping was counted for 1 min at RT using a fluorescence microscope. Wild-type N2, mutants and transgenic worms were analyzed. The data were expressed as PPM (pumps per minute).

### Life-span assay

Eggs laid by adult mother worms were synchronously grown up to the L4 larval stage on NGM plates seeded with *E. coli* OP50 at 20°C. The L4-stage worms were transferred to NGM plates containing 100 mM 5-fluoro-2'-deoxyuridine (Sigma-Aldrich, F0503) to prevent them from producing progeny. The number of worms that were alive or dead was recorded every one or 2 d. Worms that ruptured, burrowed, or crawled off the plates were censored but included in the life-span analysis as censored animals. The survival data were analyzed by using OASIS (online application for the survival analysis of life-span assays <http://sbi.postech.ac.kr/oasis/surv/>).<sup>35</sup>

### Statistical analysis

All experiments were performed blind-coded and repeated at least 3 times. The values in the figures are expressed as mean ± SEM. Differences were considered significant if *P* values were < 0.05. The graphs were drawn using Prism 5 software (Graphpad Software Inc., San Diego, CA, USA). Values were compared by one-way ANOVA with the Tukey post-hoc test using InStat (version 3.05) software (Graphpad Software Inc., San Diego, CA, USA).

### Abbreviations

ACTB	actin, $\beta$
AD	Alzheimer disease
A $\beta$	amyloid $\beta$
ALS	amyotrophic lateral sclerosis
BiFC	bimolecular fluorescence complementation
GlcNAc	<i>N</i> -acetylglucosamine
PD	Parkinson disease

$P_{myo-2}$  *myo-2* promoter  
 $P_{flp-21}$  *flp-21* promoter  
 PCR polymerase chain reaction  
 SNCA synuclein,  $\alpha$   
 TFEB transcription factor EB

## Disclosure of potential conflicts of interest

No potential conflicts of interest were disclosed.

## Funding

This work was supported by the National Research Foundation (NRF) grant funded by the Korean Government (MEST) (NRF-2015R1A2A1A10052540, NRF-2015R1A2A1A15053661), and the Korea Health Technology R&D Project, Ministry of Health & Welfare, Republic of Korea (HI14C0093), as well as the 2014 KU Brain Pool Program of Konkuk University.

## References

- Brundin P, Melki R, Kopito R. Prion-like transmission of protein aggregates in neurodegenerative diseases. *Nat Rev Mol Cell Biol* 2010; 11:301-7; PMID:20308987; <http://dx.doi.org/10.1038/nrm2873>
- Lee SJ, Desplats P, Sigurdson C, Tsigelny I, Masliah E. Cell-to-cell transmission of non-prion protein aggregates. *Nat Rev Neurol* 2010; 6:702-6; PMID:21045796; <http://dx.doi.org/10.1038/nrneurol.2010.145>
- Jucker M, Walker LC. Self-propagation of pathogenic protein aggregates in neurodegenerative diseases. *Nature* 2013; 501:45-51; PMID:24005412; <http://dx.doi.org/10.1038/nature12481>
- Bae EJ, Lee HJ, Rockenstein E, Ho DH, Park EB, Yang NY, Desplats P, Masliah E, Lee SJ. Antibody-aided clearance of extracellular  $\alpha$ -synuclein prevents cell-to-cell aggregate transmission. *J Neurosci* 2012; 32:13454-69; PMID:23015436; <http://dx.doi.org/10.1523/JNEUROSCI.1292-12.2012>
- Tran HT, Chung CH, Iba M, Zhang B, Trojanowski JQ, Luk KC, Lee VM. Alpha-synuclein immunotherapy blocks uptake and templated propagation of misfolded  $\alpha$ -synuclein and neurodegeneration. *Cell Rep* 2014; 7:2054-65; PMID:24931606; <http://dx.doi.org/10.1016/j.celrep.2014.05.033>
- Lee HJ, Bae EJ, Lee SJ. Extracellular  $\alpha$ -synuclein—a novel and crucial factor in Lewy body diseases. *Nat Rev Neurol* 2014; 10:92-8; PMID:24468877; <http://dx.doi.org/10.1038/nrneurol.2013.275>
- Outeiro TF, Putcha P, Tetzlaff JE, Spoelgen R, Koker M, Carvalho F, Hyman BT, McLean PJ. Formation of toxic oligomeric  $\alpha$ -synuclein species in living cells. *PLoS One* 2008; 3:e1867; PMID:18382657; <http://dx.doi.org/10.1371/journal.pone.0001867>
- McKay JP, Raizen DM, Gottschalk A, Schafer WR, Avery L. eat-2 and eat-18 are required for nicotinic neurotransmission in the *Caenorhabditis elegans* pharynx. *Genetics* 2004; 166:161-9; PMID:15020415; <http://dx.doi.org/10.1534/genetics.166.1.161>
- Rogers C, Reale V, Kim K, Chatwin H, Li C, Evans P, de Bono M. Inhibition of *Caenorhabditis elegans* social feeding by FMR1-related peptide activation of NPR-1. *Nat Neurosci* 2003; 6:1178-85; PMID:14555955; <http://dx.doi.org/10.1038/nn1140>
- Lee HJ, Bae EJ, Jang A, Ho DH, Cho ED, Suk JE, Yun YM, Lee SJ. Enzyme-linked immunosorbent assays for  $\alpha$ -synuclein with species and multimeric state specificities. *J Neurosci Methods* 2011; 199:249-57; PMID:21658411; <http://dx.doi.org/10.1016/j.jneumeth.2011.05.020>
- Kenyon C, Chang J, Gensch E, Rudner A, Tabtiang R. A *C. elegans* mutant that lives twice as long as wild type. *Nature* 1993; 366:461-4; PMID:8247153; <http://dx.doi.org/10.1038/366461a0>
- Denzel MS, Storm NJ, Gutschmidt A, Baddi R, Hinze Y, Jarosch E, Sommer T, Hoppe T, Antebi A. Hexosamine pathway metabolites enhance protein quality control and prolong life. *Cell* 2014; 156:1167-78; PMID:24630720; <http://dx.doi.org/10.1016/j.cell.2014.01.061>
- Vaikath NN, Majbour NK, Paleologou KE, Ardah MT, van Dam E, van de Berg WD, Forrest SL, Parkkinen L, Gai WP, Hattori N, et al. Generation and characterization of novel conformation-specific monoclonal antibodies for  $\alpha$ -synuclein pathology. *Neurobiol Dis* 2015; 79:81-99; PMID:25937088; <http://dx.doi.org/10.1016/j.nbd.2015.04.009>
- Lapierre LR, De Magalhaes Filho CD, McQuary PR, Chu CC, Visvikis O, Chang JT, Gelino S, Ong B, Davis AE, Irazoqui JE, et al. The TFEB orthologue HLH-30 regulates autophagy and modulates longevity in *Caenorhabditis elegans*. *Nat Commun* 2013; 4:2267; PMID:23925298
- Vilchez D, Morante I, Liu Z, Douglas PM, Merkwirth C, Rodrigues AP, Manning G, Dillin A. RPN-6 determines *C. elegans* longevity under proteotoxic stress conditions. *Nature* 2012; 489:263-8; PMID:22922647; <http://dx.doi.org/10.1038/nature11315>
- Hansen C, Angot E, Bergstrom AL, Steiner JA, Pieri L, Paul G, Outeiro TF, Melki R, Kallunki P, Fog K, et al.  $\alpha$ -Synuclein propagates from mouse brain to grafted dopaminergic neurons and seeds aggregation in cultured human cells. *J Clin Invest* 2011; 121:715-25; PMID:21245577; <http://dx.doi.org/10.1172/JCI43366>
- Bae EJ, Yang NY, Song M, Lee CS, Lee JS, Jung BC, Lee HJ, Kim S, Masliah E, Sardi SP, et al. Glucocerebrosidase depletion enhances cell-to-cell transmission of  $\alpha$ -synuclein. *Nat Commun* 2014; 5:4755; PMID:25156829; <http://dx.doi.org/10.1038/ncomms5755>
- Lee HJ, Suk JE, Bae EJ, Lee JH, Paik SR, Lee SJ. Assembly-dependent endocytosis and clearance of extracellular  $\alpha$ -synuclein. *Int J Biochem Cell Biol* 2008; 40:1835-49; PMID:18291704; <http://dx.doi.org/10.1016/j.biocel.2008.01.017>
- Desplats P, Lee HJ, Bae EJ, Patrick C, Rockenstein E, Crews L, Spencer B, Masliah E, Lee SJ. Inclusion formation and neuronal cell death through neuron-to-neuron transmission of  $\alpha$ -synuclein. *Proc Natl Acad Sci U S A* 2009; 106:13010-5; PMID:19651612; <http://dx.doi.org/10.1073/pnas.0903691106>
- Clark SG, Shurland DL, Meyerowitz EM, Bargmann CI, van der Blik AM. A dynamin GTPase mutation causes a rapid and reversible temperature-inducible locomotion defect in *C. elegans*. *Proc Natl Acad Sci U S A* 1997; 94:10438-43; PMID:9294229; <http://dx.doi.org/10.1073/pnas.94.19.10438>
- Lee HJ, Cho ED, Lee KW, Kim JH, Cho SG, Lee SJ. Autophagic failure promotes the exocytosis and intercellular transfer of  $\alpha$ -synuclein. *Exp Mol Med* 2013; 45:e22; PMID:23661100; <http://dx.doi.org/10.1038/emm.2013.45>
- Syntichaki P, Xu K, Driscoll M, Tavernarakis N. Specific aspartyl and calpain proteases are required for neurodegeneration in *C. elegans*. *Nature* 2002; 419:939-44; PMID:12410314; <http://dx.doi.org/10.1038/nature01108>
- Sardiello M, Palmieri M, di Ronza A, Medina DL, Valenza M, Genarino VA, Di Malta C, Donaudy F, Embrione V, Polishchuk RS, et al. A gene network regulating lysosomal biogenesis and function. *Science* 2009; 325:473-7; PMID:19556463
- Grove CA, De Masi F, Barrasa MI, Newburger DE, Alkema MJ, Bulyk ML, Walhout AJ. A multiparameter network reveals extensive divergence between *C. elegans* bHLH transcription factors. *Cell* 2009; 138:314-27; PMID:19632181; <http://dx.doi.org/10.1016/j.cell.2009.04.058>
- Klucken J, Poehler AM, Ebrahimi-Fakhari D, Schneider J, Nuber S, Rockenstein E, Schlotzer-Schrehardt U, Hyman BT, McLean PJ, Masliah E, et al. Alpha-synuclein aggregation involves a bafilomycin A 1-sensitive autophagy pathway. *Autophagy* 2012; 8:754-66; PMID:22647715; <http://dx.doi.org/10.4161/auto.19371>
- Yu WH, Dorado B, Figueroa HY, Wang L, Planel E, Cookson MR, Clark LN, Duff KE. Metabolic activity determines efficacy of macroautophagic clearance of pathological oligomeric  $\alpha$ -synuclein. *Am J Pathol* 2009; 175:736-47; PMID:19628769; <http://dx.doi.org/10.2353/ajpath.2009.080928>
- Kilpatrick K, Zeng Y, Hancock T, Segatori L. Genetic and chemical activation of TFEB mediates clearance of aggregated  $\alpha$ -synuclein. *PLoS one* 2015; 10:e0120819; PMID:25790376; <http://dx.doi.org/10.1371/journal.pone.0120819>
- Lee HJ, Khoshaghideh F, Patel S, Lee SJ. Clearance of  $\alpha$ -synuclein oligomeric intermediates via the lysosomal degradation pathway. *J Neurosci* 2004; 24:1888-96; PMID:14985429; <http://dx.doi.org/10.1523/JNEUROSCI.3809-03.2004>

- [29] Brenner S. The genetics of *Caenorhabditis elegans*. *Genetics* 1974; 77:71-94; PMID:4366476
- [30] Gengyo-Ando K, Yoshina S, Inoue H, Mitani S. An efficient transgenic system by TA cloning vectors and RNAi for *C. elegans*. *Biochem Biophys Res Commun* 2006; 349:1345-50; PMID:16979594; <http://dx.doi.org/10.1016/j.bbrc.2006.08.183>
- [31] Lee LW, Lo HW, Lo SJ. Vectors for co-expression of two genes in *Caenorhabditis elegans*. *Gene* 2010; 455:16-21; PMID:20149852; <http://dx.doi.org/10.1016/j.gene.2010.02.001>
- [32] Hobert O. PCR fusion-based approach to create reporter gene constructs for expression analysis in transgenic *C. elegans*. *BioTechniques* 2002; 32:728-30; PMID:11962590
- [33] Mello CC, Kramer JM, Stinchcomb D, Ambros V. Efficient gene transfer in *C.elegans*: extrachromosomal maintenance and integration of transforming sequences. *EMBO J* 1991; 10:3959-70; PMID:1935914
- [34] Frokjaer-Jensen C, Davis MW, Hopkins CE, Newman BJ, Thummel JM, Olesen SP, Grunnet M, Jorgensen EM. Single-copy insertion of transgenes in *Caenorhabditis elegans*. *Nat Genet* 2008; 40:1375-83; PMID:18953339; <http://dx.doi.org/10.1038/ng.248>
- [35] Yang JS, Nam HJ, Seo M, Han SK, Choi Y, Nam HG, Lee SJ, Kim S. OASIS: online application for the survival analysis of lifespan assays performed in aging research. *PloS one* 2011; 6:e23525; PMID:21858155; <http://dx.doi.org/10.1371/journal.pone.0023525>